

# Organic Structure-Directing Agent-Free Synthesis of Mordenite-Type Zeolites Driven by Al-Rich Amorphous Aluminosilicates

Ting Xiao, Mizuho Yabushita,\* Toshiki Nishitoba, Ryota Osuga, Motohiro Yoshida, Masaki Matsubara, Sachiko Maki, Kiyoshi Kanie, Toshiyuki Yokoi, Wenbin Cao, and Atsushi Muramatsu\*



Cite This: *ACS Omega* 2021, 6, 5176–5182



Read Online

ACCESS |



Metrics & More

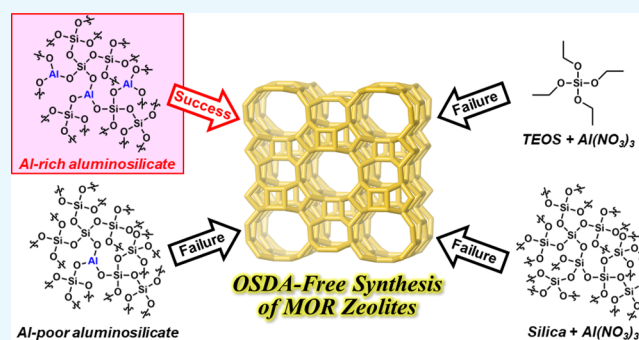


Article Recommendations



Supporting Information

**ABSTRACT:** Mordenite (MOR)-type zeolites with a Si/Al molar ratio of up to 13 with crystallite sizes of ca. 60 nm were successfully synthesized from Al-rich aluminosilicates with a Si/Al ratio of 2 and additional SiO<sub>2</sub> under seed-assisted hydrothermal conditions for 6 h or longer without any organic structure-directing agents (OSDAs). In stark contrast, under the same hydrothermal conditions for 6 h, control experiments using starting reagent(s), such as Al-poor aluminosilicate, pure SiO<sub>2</sub>, tetraethyl orthosilicate, and Al(NO<sub>3</sub>)<sub>3</sub>, all of which are typically employed for zeolite synthesis, failed to yield MOR-type zeolites. The penta-coordinated Al species, which are present in Al-rich aluminosilicates and are more reactive than the tetra- and hexa-coordinated Al species typically found in alumina and Al-poor aluminosilicates, played a decisive role in the OSDA-free synthesis of MOR-type zeolites.



## INTRODUCTION

Crystalline and porous aluminosilicates, so-called zeolites, have been recognized as attractive functional materials, and they are indeed used widely in the chemical industry.<sup>1–5</sup> Conventional techniques to synthesize zeolites rely on the use of organic structure-directing agents (OSDAs) as templates to form the desired porous structure under hydrothermal conditions.<sup>2,5,6</sup> However, such processes inevitably present problems such as high cost and a high E-factor. Furthermore, an energy-consuming postsynthetic calcination treatment is necessary to remove OSDA molecules completely from zeolites, which is sometimes accompanied by the distortion of the zeolite framework as a result of steam produced during the combustion of OSDAs.<sup>7,8</sup> Thus, the development of low-cost, environmentally benign, and direct methods for synthesizing zeolites without OSDAs is highly desired, and to date, a variety of zeolite frameworks have been successfully synthesized under OSDA-free conditions.<sup>9–12</sup>

Mordenite (MOR)-type zeolites are known to be effective catalysts for cracking, reforming, hydroisomerization, alkylation, and dewaxing, as well as good adsorbents.<sup>13–15</sup> The OSDA-free synthesis of MOR-type zeolites has been achieved under various hydrothermal conditions,<sup>16–21</sup> yet the Si/Al molar ratios of the resulting MOR zeolites have typically been within the range of  $\leq 10$ .<sup>16–20</sup> From the perspective of thermal stability, high-silica zeolite frameworks are advantageous over low-silica ones.<sup>22,23</sup> In addition, the enhanced hydrophobicity of high-silica zeolites because of their low Al content has been

demonstrated to be beneficial to some catalytic reactions.<sup>24</sup> The OSDA-free and direct synthesis of high-silica MOR-type zeolites, therefore, is promising and has been developed under carefully controlled hydrothermal conditions using various types of SiO<sub>2</sub> and NaAlO<sub>2</sub> as sources of Si and Al, respectively, in the presence/absence of seed crystals.<sup>25–27</sup>

In this manuscript, a different approach to achieve the OSDA-free synthesis of high-silica MOR-type zeolites was demonstrated, where Al-rich amorphous aluminosilicates were employed as sources of both Si and Al. The motivation to use Al-rich precursors arose from the higher reactivity of the penta-coordinated Al species as compared to that of the tetra- and hexa-coordinated Al species typically found in aluminas and aluminosilicates.<sup>28</sup> According to a previous report, a penta-coordinated Al content was enriched upon the decrease in a Si/Al molar ratio.<sup>29</sup> Thus, Al-rich aluminosilicates involving penta-coordinated Al species may readily undergo dissolution in the presence of bases, and the dissolved species may offer a unique opportunity to construct zeolite frameworks.

Received: October 16, 2020

Accepted: February 9, 2021

Published: February 16, 2021



Table 1. Effects of Synthesis Parameters on Hydrothermally Prepared Samples

sample	starting material(s)	synthesis parameters			product information				
		Si/Al <sup>a</sup>	aging time /h	HT temp. <sup>b</sup> /°C	HT time <sup>c</sup> /h	phase(s) <sup>d</sup>	D <sup>e</sup> /nm	Si/Al <sup>f</sup>	yield <sup>g</sup> /%
M1	TEOS, Al(NO <sub>3</sub> ) <sub>3</sub>	20	48	160	6	amorphous	—	14	n.d. <sup>h</sup>
M2	SiO <sub>2</sub> , Al(NO <sub>3</sub> ) <sub>3</sub>	20	48	160	6	amorphous	—	12	n.d. <sup>h</sup>
M3	AP2, SiO <sub>2</sub>	20	48	160	6	MOR	51	7.3	42
M4 <sup>i</sup>	AP2, SiO <sub>2</sub>	20	48	160	6	amorphous	—	9.8	47
M5	AP20	20	48	160	6	MOR, amorphous	32	9.4	51
M6	AP, Al(NO <sub>3</sub> ) <sub>3</sub>	20	48	160	6	amorphous	—	12	n.d. <sup>h</sup>
M7	AP2, SiO <sub>2</sub>	20	48	160	3	amorphous	—	7.9	39
M8	AP2, SiO <sub>2</sub>	20	48	160	5	amorphous	—	8.1	39
M9	AP2, SiO <sub>2</sub>	20	48	160	24	MOR	58	7.4	43
M10	AP2, SiO <sub>2</sub>	20	48	160	72	MOR	59	10	51
M11	AP2, SiO <sub>2</sub>	20	48	160	120	MOR	56	13	51
M12	AP2, SiO <sub>2</sub>	20	48	120	6	amorphous	—	8.4	39
M13	AP2, SiO <sub>2</sub>	20	48	140	6	MOR, amorphous	59	8.7	40
M14	AP2, SiO <sub>2</sub>	20	6	160	6	MOR, amorphous	35	8.5	37
M15	AP2, SiO <sub>2</sub>	20	24	160	6	MOR, amorphous	44	7.6	39
M16	AP2, SiO <sub>2</sub>	5	48	160	120	MOR, ANA	60	3.7	88
M17	AP2, SiO <sub>2</sub>	10	48	160	120	MOR	62	5.8	68

<sup>a</sup>Si/Al molar ratio of synthesis gel excluding the seed (see the Experimental Section). <sup>b</sup>Temperature of the hydrothermal treatment. <sup>c</sup>Time of the hydrothermal treatment. <sup>d</sup>Elucidated by the XRD patterns in Figures 1 and 3, and Figures S4–S6. <sup>e</sup>Crystallite size of MOR-type zeolite, determined by applying the Scherrer equation to the 202 reflection at  $2\theta$  of 25.8°. <sup>f</sup>Actual Si/Al molar ratio of the synthesized samples, elucidated by inductively coupled plasma–atomic emission spectroscopy (ICP–AES). <sup>g</sup>Yield of the solid product, calculated by dividing the mass of the dried solid product by the total mass of the dried solid reagents (i.e., (alumino)silicate, SiO<sub>2</sub>, and MOR seed). <sup>h</sup>Not determined due to the use of homogeneous starting reagent(s). <sup>i</sup>The hydrothermal process was conducted without the MOR seed.

## RESULTS AND DISCUSSION

Prior to the zeolite synthesis, three (alumino)silicates, denoted as AP (pure SiO<sub>2</sub> without Al atoms), AP2 (Si/Al molar ratio: 2), and AP20 (Si/Al molar ratio: 20), were prepared via a polymerized complex method to achieve atomic-level homogeneity<sup>30</sup> (see the Experimental Section). The X-ray diffraction (XRD) patterns for all three of these (alumino)silicates featured a broad halo at ca. 22°, indicating that all of them were amorphous (see Figure S1 and Table S1 in the Supporting Information). These (alumino)silicates were subsequently employed in the hydrothermal synthesis as the starting reagents. Under OSDA-free conditions, the effects of various synthesis parameters—the class of starting material(s), hydrothermal treatment conditions, the Si/Al molar ratio, and the aging time at room temperature—on the formation of the MOR-type framework were investigated because these parameters are well known to affect synthesis processes as well as the textural properties of the resulting products.<sup>2,5</sup> The resulting phase(s), crystallite sizes, Si/Al molar ratios, and the yield of the solid product are tabulated in Table 1.

Initially, a variety of starting reagents were employed for the hydrothermal process to investigate whether MOR-type zeolites could be formed in each case. The hydrothermal processes for 6 h using the homogeneous starting reagents such as tetraethyl orthosilicate (TEOS) and Al(NO<sub>3</sub>)<sub>3</sub> did not yield a MOR-type zeolite, but rather provided amorphous products with atypical morphology (Figure S2), as evidenced by the fact that only a broad halo was observed in their XRD patterns at ca. 22° (see M1 and M2 in Table 1 and Figure 1). In stark contrast, the combination of an amorphous aluminosilicate with a Si/Al ratio of 2 (i.e., AP2) and additional SiO<sub>2</sub>, the latter of which was used to control the Al concentration in the synthesis gel to 20 before the addition of the seed, successfully yielded a platelike MOR-type zeolite under the same hydrothermal conditions (see M3 in Table 1

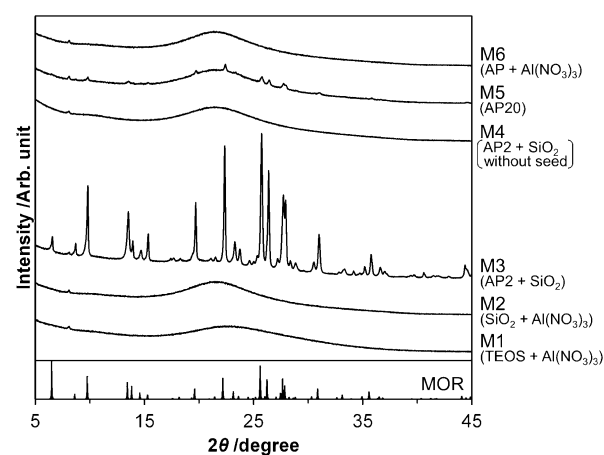
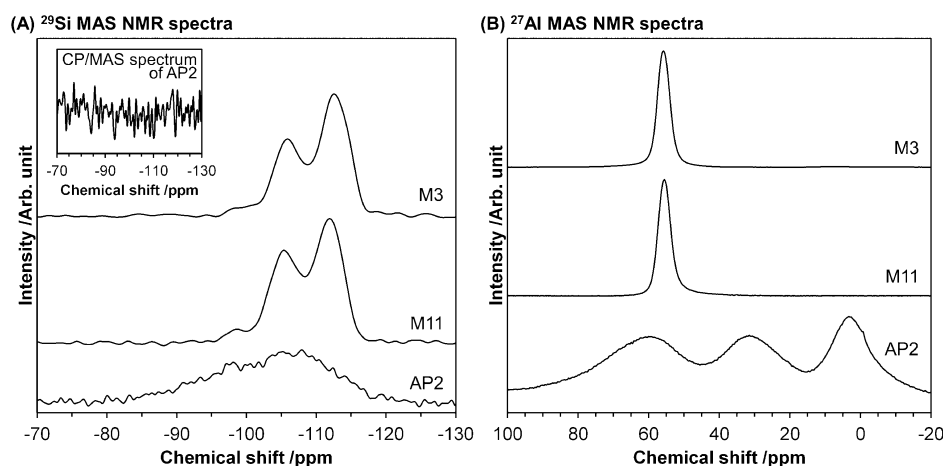
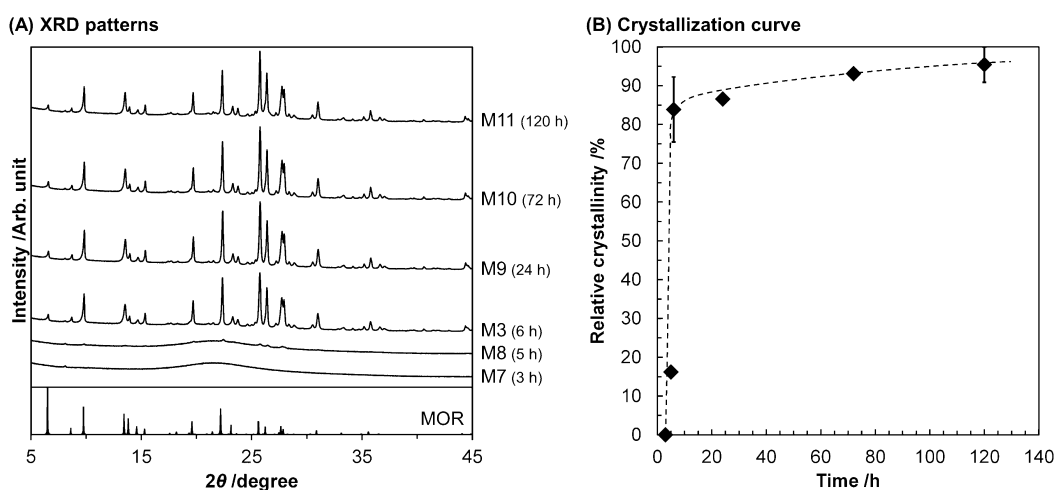


Figure 1. Effects of starting reagent(s) on the solid product, as confirmed by XRD measurements. The sample denotation is given in Table 1. The information in parentheses shows the starting reagent(s) used. The reference pattern for MOR is from the database provided by International Zeolite Association (IZA), adopted with permission from Baerlocher, C; McCusker, L. B. Database of Zeolite Structures. <http://www.iza-structure.org/databases/> (accessed Jan 1, 2021).<sup>31</sup>

and Figure 1 and Figure S2). Given that the hydrothermal process without the MOR seed failed to yield the MOR-type zeolites (see M4 in Table 1 and Figure 1), the MOR seed is responsible for the construction of the MOR-type zeolite framework under the OSDA-free conditions. The crystallite size was calculated to be 51 nm by applying the Scherrer equation to the 202 reflection at  $2\theta$  of 25.8°,<sup>31</sup> which was comparable or even smaller, relative to the previously reported MOR crystals that were prepared under the OSDA-free conditions.<sup>17,21,25</sup> Such a small crystallite size is beneficial for catalysis because the substrate molecules gain easy access to the active sites mainly located inside the zeolite crystals owing



**Figure 2.** Nature of the Si and Al species contained in AP2, M3, and M11, as revealed by (A)  $^{29}\text{Si}$  MAS NMR spectroscopy (inset shows the  $^{29}\text{Si}$  CP/MAS NMR spectrum of AP2) and (B)  $^{27}\text{Al}$  MAS NMR spectroscopy.



**Figure 3.** (A) Effects of the duration of hydrothermal treatment on the crystallization process and (B) crystallization curve for the synthesis of MOR-type zeolites from AP2 and additional  $\text{SiO}_2$ . The reference pattern for MOR is from the database provided by IZA, adopted with permission from Baerlocher, C; McCusker, L. B. Database of Zeolite Structures. <http://www.iza-structure.org/databases/> (accessed Jan 1, 2021).<sup>31</sup> The relative crystallinity was elucidated by comparing the peak height at  $2\theta$  of  $25.8^\circ$  (the 202 reflection)<sup>31</sup> of the MOR-type zeolite synthesized via the hydrothermal process for 120 h and that of each MOR sample (i.e., the value of 100% was defined by the upper limit of the data point at 120 h).

to a short diffusion path length.<sup>6,32,33</sup> The Si/Al ratio of the obtained MOR zeolite was determined by inductively coupled plasma–atomic emission spectroscopy (ICP–AES) to be 7.3, which was 2.9 times lower than the value expected on the basis of the loading amounts of the starting reagents including the seed (i.e., 21, see the Experimental Section). This difference indicates that AP2 was transformed into the resulting MOR zeolite with the incorporation of a small amount of the Si-containing species derived from additional  $\text{SiO}_2$ , most of which remained dissolved in the liquid phase.  $^{29}\text{Si}$  magic angle spinning nuclear magnetic resonance (MAS NMR) spectroscopy revealed the presence of Si species assignable to  $\text{Q}^4(0\text{Al})$  (–113 ppm),  $\text{Q}^4(1\text{Al})$  (–106 ppm), and  $\text{Q}^4(2\text{Al})$  (–100 ppm), where  $\text{Q}^4(n\text{Al})$  represents the  $\text{Si}(\text{OSi})_{4-n}(\text{OAl})_n$  ( $0 \leq n \leq 4$ ) species (Figure 2A).<sup>34,35</sup> The characteristic peak at 56 ppm in the  $^{27}\text{Al}$  MAS NMR spectrum and the absence of any other peaks revealed that all the Al atoms were tetrahedrally incorporated in the MOR-type framework (Figure 2B).<sup>35,36</sup>

Although the same quantities of Si and Al were present in the synthesis gel as in M3, another control hydrothermal process for 6 h using amorphous aluminosilicate with a Si/Al

ratio of 20 (i.e., AP20) gave a mixture of amorphous material and a small amount of MOR (see M5 in Table 1 and Figure 1). Likewise, the combination of pure silica prepared via a polymerized complex method (i.e., AP) and using homogeneous  $\text{Al}(\text{NO}_3)_3$  yielded an amorphous solid (see M6 in Table 1 and Figure 1). These data demonstrated that the Al content of the amorphous aluminosilicates was key in the construction of the MOR-type zeolite framework under the OSDA-free and seed-assisted conditions. AP2 presumably consists of relatively unstable and reactive species, and thus, it easily undergoes hydrolysis under the hydrothermal conditions to generate soluble complexes containing Al atoms, which then act as the building blocks of a zeolite framework, in contrast to the Al-poor aluminosilicate AP20.

The broad resonance seen in the  $^{29}\text{Si}$  MAS NMR spectrum of AP2 (Figure 2A), which is typical of amorphous or highly disordered aluminosilicates,<sup>37</sup> demonstrated the presence of five different Si species, viz.,  $\text{Q}^4(0\text{Al})$  at –115 ppm,  $\text{Q}^4(1\text{Al})$  at –108 ppm,  $\text{Q}^4(2\text{Al})$  at –102 ppm,  $\text{Q}^4(3\text{Al})$  at –95.7 ppm, and  $\text{Q}^4(4\text{Al})$  at –87.5 ppm, respectively.<sup>36</sup> Note that AP2 did not contain any  $\text{Q}^m(n\text{Al})$  species (i.e., Si-

$(\text{OSi})_{4-n-m}(\text{OAl})_n(\text{OH})_m$  ( $0 \leq n \leq 3$ ,  $1 \leq m \leq 3$ ), given that no peaks were detected in the  $^{29}\text{Si}$  cross-polarization (CP)/MAS NMR spectrum (see the inset of Figure 2A). The Fourier-transform infrared (FT-IR) spectrum of AP2 also demonstrated a lack of OH groups in AP2 because no absorption band was observed in the wavenumber range of 3800–3200  $\text{cm}^{-1}$  (Figure S1). At the last stage of AP2 preparation (see the Experimental Section), the aluminosilicate-carbon composite was calcined at a high temperature of 800 °C to remove the carbonized material, which should simultaneously eliminate OH groups from the resulting AP2. The  $^{27}\text{Al}$  MAS NMR spectrum of AP2 indicated that the tetra-, penta-, and hexa-coordinated Al atoms, which were observed at 60, 30, and 0 ppm, respectively,<sup>36,38</sup> were present in its structure (Figure 2B). According to a previous report, penta-coordinated Al atoms undergo dissolution more readily than tetra- and hexa-coordinated ones,<sup>28</sup> suggesting that the penta-coordinated Al species in AP2 play a decisive role in the OSDA-free synthesis of MOR-type zeolites.

To explore the crystallization process for OSDA-free and seed-assisted MOR-type zeolite synthesis from AP2, the duration of the hydrothermal treatment was varied from 5 to 120 h at 160 °C. Figure 3 shows the crystallization curve for the MOR synthesis, obtained from the corresponding XRD patterns (see also M3 and M7–M11 in Table 1). The hydrothermal treatment for 3 h did not convert any AP2 into MOR zeolite. As the treatment time was prolonged to 5 h, small diffraction peaks due to MOR zeolite appeared, along with an amorphous phase derived from AP2 and additional  $\text{SiO}_2$ . These results indicated that a 5 h or shorter hydrothermal treatment was inefficient to crystallize the MOR-type zeolite. Crystallization proceeded rapidly between 5–6 h and was completed at 72 h. Once the relative crystallinity reached >90%, the solid yield did not increase anymore, and the relative crystallinity was altered to some extent in the narrow range of 90–100% (see Table 1 and Figure 3). The crystallization curve and significant difference of particle sizes between AP2 and the MOR-type zeolites (see Figures S1 and S3) suggest that the (alumino)silicate molecules are generated through the solid–liquid equilibrium-controlled dissolution from AP2 and  $\text{SiO}_2$  in the induction period within 5 h, and the formation of nuclei from these dissolved species and the crystal growth proceed subsequently.<sup>39,40</sup> Another pathway of crystallization consisting of the attachment of amorphous particles to the crystal surfaces and subsequent direct transformation into both nuclei and crystals is also possible.<sup>41</sup> This mechanism is supported by the fast consumption of large particles at the hydrothermal duration time between 5–6 h as well as by the formation of irregular-shaped particles of the MOR-type zeolites (Figure S3). Consequently, the data shown here suggest that these two crystal growth mechanisms, the step-by-step addition of dissolved species as well as the attachment of particles, simultaneously proceeded. Another important result is the gradual increase in the Si/Al ratio with an elapsed treatment time, indicating that the Si species supplied from the additional  $\text{SiO}_2$  were gradually incorporated into the MOR crystals probably via the same mechanism as alluded to above, and the highest Si/Al ratio achieved in this study was 13 (see M11 in Table 1).  $^{29}\text{Si}$  and  $^{27}\text{Al}$  MAS NMR spectroscopy revealed the presence of Si species consisting of  $\text{Q}^4(\text{0Al})$ ,  $\text{Q}^4(\text{1Al})$ , and  $\text{Q}^4(\text{2Al})$  and Al species tetrahedrally incorporated in the

zeolite framework in the M11 sample (see Figure 2), consistent with M3.

The effects of other synthesis parameters—temperature of the hydrothermal treatment, duration of aging at room temperature, and Si/Al ratio based on the loading amounts of starting reagents—were investigated at the hydrothermal treatment time of 6 h, which is the shortest time to obtain MOR-type zeolites with good crystallinity (vide supra) because a short synthesis time is beneficial in terms of the industrial applications of zeolites. In the XRD patterns for M12 and M13, which were hydrothermally synthesized for 6 h at 120 and 140 °C, respectively, a broad halo was observed at 22°, along with almost negligible peaks derived from the MOR phase in the case of M13 (see Table 1 and Figure S4). These results clearly demonstrated that temperatures below 160 °C are not enough to transform AP2 into an MOR-type zeolite in the same reaction time (6 h), as the successful case of M3 prepared at 160 °C. At lower temperatures, the dissolution of AP2 into the reaction media did not proceed readily, which is a prerequisite for the crystallization of zeolites. This could be the reason why an MOR zeolite was not formed under lower-temperature conditions. Presumably because of the same reason as for the dissolution, aging times also affected the resulting phases significantly, and the degree of crystallization of the MOR zeolites increased as the aging time increased from 6 to 48 h (see M3, M14, and M15 in Table 1 and Figure S5). The effects of the Si/Al ratios of the synthesis gel on the OSDA-free hydrothermal process to synthesize MOR-type zeolites were also examined (see M3, M16, and M17 in Table 1 and Figure S6). Single-phase MOR-type zeolites with the actual Si/Al ratios of 7.3 and 5.8 were successfully prepared from synthesis gels with the initial Si/Al ratios excluding the MOR seed of 20 and 10, respectively, while a lower initial Si/Al ratio excluding the seed of 5 yielded a mixture of the MOR zeolite and an impurity that was identified as the analcime (ANA)-type zeolite, in agreement with the previous reports.<sup>25,31,42</sup> These differences indicated that a synthesis gel with a very high Al content led to the formation of a zeolite framework of another class as a byproduct.

The synthesis of another class of the framework topology, Zeolite Socony Mobil-five (MFI)-type zeolites, from the Al-rich aluminosilicate (i.e., AP2) under the OSDA-free and seed-assisted hydrothermal conditions was further examined. As evidenced by the XRD patterns shown in Figure 4, the MFI-type framework was constructed at the Si/Al ratios of 11 and 27, the values of which were determined by the ICP–AES measurements. Consistent with the cases of MOR-type zeolites (vide supra),  $^{27}\text{Al}$  MAS NMR spectroscopy demonstrated the presence of Al tetrahedra in the MFI-type framework, without any extra-framework Al species (Figure S8). These data indicated that the OSDA-free approach using the Al-rich aluminosilicates demonstrated here has a potential to be widely applicable to synthesizing a variety of zeolite topologies.

## CONCLUSIONS

Seed-assisted hydrothermal processes using Al-rich amorphous aluminosilicates with a Si/Al molar ratio of 2 and additional  $\text{SiO}_2$  as starting reagents offered a unique opportunity to synthesize MOR-type zeolites with the Si/Al ratios of up to 13 with the crystallite sizes as small as ca. 60 nm without any OSDAs. The present hydrothermal syntheses, performed under a variety of conditions, have demonstrated that amorphous aluminosilicates must have a high Al content if

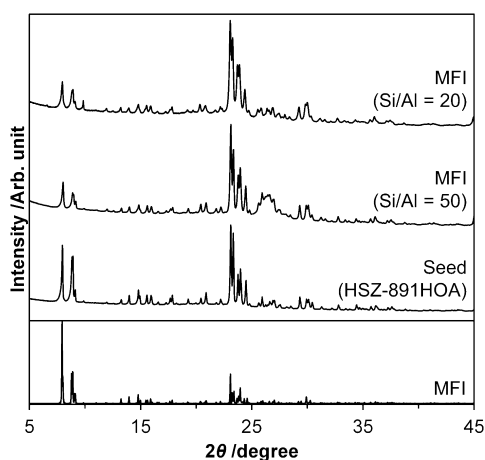


**Figure 4.** XRD patterns of solid products synthesized hydrothermally using the MFI seed and synthesis gels with different Si/Al ratios. The values in the parentheses are the Si/Al ratios of the synthesis gels excluding the seed (see the [Experimental Section](#)) and the actual Si/Al ratios determined by ICP–AES were 11 and 27, respectively. The reference pattern for MFI is from the database provided by IZA, adopted with permission from Baerlocher, C; McCusker, L. B. Database of Zeolite Structures. <http://www.iza-structure.org/databases/> (accessed Jan 1, 2021).<sup>31</sup>

they are able to function as precursors to the OSDA-free synthesis of high-silica MOR-type zeolites. The key factor is the presence in the Al-rich amorphous aluminosilicates of penta-coordinated Al species, which are more reactive than the other Al species typically found in other Al-containing oxides.<sup>28</sup> The experimental data obtained in the present work suggest that the use of Al-rich amorphous aluminosilicates could pave the way for the synthesis of a variety of zeolite frameworks even under the OSDA-free conditions as well as for the design of new functional materials.

## ■ EXPERIMENTAL SECTION

**Reagents.** The following reagents were used as received to synthesize amorphous (alumino)silicates and MOR-type zeolites: TEOS (Kojundo Chemical Laboratory); propylene glycol (PG; FUJIFILM Wako Pure Chemical); an aqueous HNO<sub>3</sub> solution (1 M, FUJIFILM Wako Pure Chemical), Al(NO<sub>3</sub>)<sub>3</sub>•9H<sub>2</sub>O (FUJIFILM Wako Pure Chemical); citric acid (CA; anhydrous, Nacalai Tesque); ethylene glycol (EG; FUJIFILM Wako Pure Chemical); silica gel (Carplex BS-304F, DSL, Japan); and an aqueous NaOH solution (8 M, FUJIFILM Wako Pure Chemical). For the quantitative analysis of Si and Al atoms contained in each specimen, an aqueous HF solution (50%, FUJIFILM Wako Pure Chemical) was used.

**Synthesis of Amorphous (Alumino)silicates via the Polymerized Complex Method.** The amorphous (alumino)silicates that were employed as precursors to zeolites were prepared by the so-called polymerized complex method.<sup>30</sup> To avoid undesired evaporation and the hydrolysis of TEOS during the preparation procedure, first, propylene glycol-modified silane (PGMS) was synthesized.<sup>43</sup> Thus, a mixture of 0.1 mol of TEOS and 0.4 mol of propylene glycol was stirred at 80 °C for 24 h, followed by the addition of 1 mL of a 1 M aqueous solution of HNO<sub>3</sub> and further stirring at the same temperature for 1 h. The resulting transparent and colorless solution was transferred into a 200 mL volumetric

flask and diluted with deionized water to obtain a 0.5 M aqueous solution of PGMS.

Afterward, the thus-prepared PGMS, Al(NO<sub>3</sub>)<sub>3</sub>•9H<sub>2</sub>O, CA, and EG were mixed at the molar ratios of 2/0/16/48, 2/1/16/48, and 20/1/160/480 in a 500 mL beaker. The mixture was stirred at 60 °C until all solids were dissolved completely, and then, it was heated at 100 °C for 1 h to remove water. The temperature was subsequently increased to 150 °C to cause condensation between CA and EG to form a resin and gradually increased to 450 °C to carbonize the resin. The resulting black powder (i.e., (alumino)silicate-carbon composite) was calcined in air in an electric furnace at 800 °C for 12 h to remove the carbonized resin. The samples prepared from the mixtures containing PGMS, Al(NO<sub>3</sub>)<sub>3</sub>•9H<sub>2</sub>O, CA, and EG with the molar ratios of 2/0/16/48, 2/1/16/48, and 20/1/160/480 were denoted as AP, AP2, and AP20, respectively.

**OSDA-Free Synthesis of MOR-Type Zeolites from Amorphous (Alumino)silicates.** The MOR-type zeolites were synthesized hydrothermally using the prepared amorphous (alumino)silicates as precursors under the OSDA-free and seed-assisted conditions. The amorphous (alumino)silicates (i.e., AP, AP2, or AP20) as a source of both Si and Al, silica as an additional Si source, an aqueous NaOH solution, and deionized water were charged into a Teflon-lined high-pressure reactor (Model 4749 General Purpose Acid Digestion Vessels, Parr Instrument Company, inner volume 23 mL) with the molar ratios of Si/Al/NaOH/H<sub>2</sub>O = 1/0.05–0.2/0.44/30. The mixture was stirred at room temperature for a designated aging time (i.e., 6, 24, or 48 h). Just before the hydrothermal treatment, a commercially available MOR zeolite (HSZ-690HOA, Tosoh, Si/Al = 120, loading amount: 5 wt % against the total weight of SiO<sub>2</sub>), whose XRD pattern is shown in [Figure S7](#), was added as a seed into the reactor. It should be noted that the actual Si/Al ratios of each synthesis gel were increased from 5, 10, and 20 to 5.2, 11, and 21, respectively, by the addition of the MOR seed. The hydrothermal reaction was carried out in an electric furnace (HIRO Company) at a tumbling speed of 10 rpm at specific temperatures and for various times. At that time, the reactor was placed into the furnace that was preheated at specific temperatures to decrease the temperature-increasing period as short as possible. After the hydrothermal process, the solid product was separated and washed with deionized water via centrifugation, dried at 60 °C overnight, and calcined at 550 °C for 12 h. The yield of the solid product was determined by dividing the mass of the dried solid product by the total mass of the dried solid reagents (i.e., (alumino)silicate, SiO<sub>2</sub>, and MOR seed).

**OSDA-Free Synthesis of MFI-Type Zeolites from AP2.** For synthesizing the MFI-type zeolites, AP2, silica, an aqueous NaOH solution, and deionized water were charged into the Teflon-lined high-pressure reactor with the molar ratios of Si/Al/NaOH/H<sub>2</sub>O = 1/0.02–0.05/0.2/30. The mixture was stirred at room temperature for 48 h. Just before the hydrothermal treatment, a commercially available MFI zeolite (HSZ-891HOA, Tosoh, Si/Al = 750, loading amount: 5 wt % against the total weight of SiO<sub>2</sub>), whose XRD pattern is shown in [Figure 4](#), was charged as a seed into the reactor. It should be noted that the actual Si/Al ratios of each synthesis gel were changed from 20 and 50 to 21 and 52, respectively, by the addition of the MFI seed. The hydrothermal reaction was carried out in the electric furnace, which was preheated at 160 °C, at a tumbling speed of 10 rpm for 120 h. After the hydrothermal process, the solid product was separated and

washed with deionized water via centrifugation, dried at 60 °C overnight, and calcined at 550 °C for 12 h, to obtain the MFI-type zeolites.

**Characterization.** The crystalline phases of the prepared samples were analyzed by powder XRD (Ultima IV, Rigaku, equipped with a semiconductor detector, Cu K $\alpha$  radiation (40 kV, 40 mA), scan speed: 2.0° min<sup>-1</sup>) with the SmartLab Studio II version 4.3.282.0 software (Rigaku). The morphology of the samples was examined by field-emission scanning electron microscopy (FE-SEM; JSM-7800 F, JEOL), with an accelerating voltage of 5 kV after Pt was sputtered onto the sample surfaces. The Si/Al molar ratios of the samples were determined by ICP–AES (SPECTRO ARCOS, AMETEK). Prior to the measurement, 50 mg of each sample was dispersed in 3 mL of an aqueous HF solution (50 wt %), and the suspension was left to stand at room temperature until the complete dissolution of the sample. After the addition of 47 mL of deionized water, the aqueous solution was further diluted 10 times in deionized water, and the resulting colorless transparent aqueous solution was analyzed by ICP–AES. Solid-state <sup>27</sup>Al MAS NMR (JNM-ECA600, JEOL, <sup>27</sup>Al 156 MHz, MAS frequency 15 kHz) and solid-state <sup>29</sup>Si MAS NMR spectroscopy (JNM-ECA600, JEOL, <sup>29</sup>Si 119 MHz, MAS frequency 15 kHz) with/without CP were employed to characterize the coordination nature of the Al and Si atoms, respectively. The NMR data were managed with the Delta/NMR version 5.0 software (JEOL). The chemical structure of AP2 was also investigated by attenuated total reflection/FT-IR spectroscopy (ATR/FT-IR; IR Affinity-1S, Shimadzu).

## ■ ASSOCIATED CONTENT

### Supporting Information

The Supporting Information is available free of charge at <https://pubs.acs.org/doi/10.1021/acsomega.0c05059>.

XRD patterns, FT-IR spectrum, SEM image, and the compositions of (alumino)silicates prepared via a polymerized complex method, SEM images and XRD patterns of solid products synthesized under various hydrothermal conditions with the MOR seed, XRD pattern of the MOR seed, and NMR spectra of the hydrothermally synthesized MFI-type zeolites (PDF).

## ■ AUTHOR INFORMATION

### Corresponding Authors

**Mizuho Yabushita** – Department of Applied Chemistry, School of Engineering, Tohoku University, Sendai, Miyagi 980-8579, Japan; [orcid.org/0000-0001-9739-0954](https://orcid.org/0000-0001-9739-0954); Email: [m.yabushita@tohoku.ac.jp](mailto:m.yabushita@tohoku.ac.jp)

**Atsushi Muramatsu** – Institute of Multidisciplinary Research for Advanced Materials and International Center for Synchrotron Radiation Innovation Smart, Tohoku University, Sendai, Miyagi 980-8577, Japan; Core Research for Evolutional Science and Technology, Japan Science and Technology Agency, Saitama 332-0012, Japan; Email: [mura@tohoku.ac.jp](mailto:mura@tohoku.ac.jp)

### Authors

**Ting Xiao** – Institute of Multidisciplinary Research for Advanced Materials, Tohoku University, Sendai, Miyagi 980-8577, Japan; Department of Inorganic Nonmetallic Materials, School of Materials Science and Engineering,

University of Science and Technology Beijing, Beijing 100083, China

**Toshiki Nishitoba** – Institute of Innovative Research, Tokyo Institute of Technology, Yokohama, Kanagawa 226-8503, Japan

**Ryota Osuga** – Institute of Multidisciplinary Research for Advanced Materials, Tohoku University, Sendai, Miyagi 980-8577, Japan

**Motohiro Yoshida** – Institute of Multidisciplinary Research for Advanced Materials, Tohoku University, Sendai, Miyagi 980-8577, Japan

**Masaki Matsubara** – Institute of Multidisciplinary Research for Advanced Materials, Tohoku University, Sendai, Miyagi 980-8577, Japan; National Institute of Technology, Sendai College, Natori, Miyagi 981-1239, Japan

**Sachiko Maki** – International Center for Synchrotron Radiation Innovation Smart, Tohoku University, Sendai, Miyagi 980-8577, Japan

**Kiyoshi Kanie** – Institute of Multidisciplinary Research for Advanced Materials and International Center for Synchrotron Radiation Innovation Smart, Tohoku University, Sendai, Miyagi 980-8577, Japan; [orcid.org/0000-0003-1477-6515](https://orcid.org/0000-0003-1477-6515)

**Toshiyuki Yokoi** – Institute of Innovative Research, Tokyo Institute of Technology, Yokohama, Kanagawa 226-8503, Japan; [orcid.org/0000-0002-3315-3172](https://orcid.org/0000-0002-3315-3172)

**Wenbin Cao** – Department of Inorganic Nonmetallic Materials, School of Materials Science and Engineering, University of Science and Technology Beijing, Beijing 100083, China

Complete contact information is available at: <https://pubs.acs.org/doi/10.1021/acsomega.0c05059>

### Notes

The authors declare no competing financial interest.

## ■ ACKNOWLEDGMENTS

This work was supported by the Core Research for Evolutional Science and Technology of the Japan Science and Technology Agency (JST CREST, Grant No. JPMJCR16P3). T.X. is grateful for the scholarship granted to a visiting Ph.D. student of the Inter-University Exchange Project by China Scholarship Council (CSC, Scholarship No. 201906460114).

## ■ REFERENCES

- (1) Corma, A. From Microporous to Mesoporous Molecular Sieve Materials and Their Use in Catalysis. *Chem. Rev.* **1997**, *97*, 2373–2420.
- (2) *Zeolites and Catalysis: Synthesis, Reactions and Applications*; Čejka, J.; Corma, A.; Zones, S., Eds.; Wiley-VCH: Weinheim, 2010.
- (3) De Clercq, R.; Dusselier, M.; Sels, B. F. Heterogeneous catalysis for bio-based polyester monomers from cellulosic biomass: advances, challenges and prospects. *Green Chem.* **2017**, *19*, S012–S040.
- (4) Prech, J.; Pizarro, P.; Serrano, D. P.; Čejka, J. From 3D to 2D zeolite catalytic materials. *Chem. Soc. Rev.* **2018**, *47*, 8263–8306.
- (5) Dusselier, M.; Davis, M. E. Small-Pore Zeolites: Synthesis and Catalysis. *Chem. Rev.* **2018**, *118*, S265–S329.
- (6) Sachse, A.; García-Martínez, J. Surfactant-Templating of Zeolites: From Design to Application. *Chem. Mater.* **2017**, *29*, 3827–3853.
- (7) Zholobenko, V.; Garforth, A.; Dwyer, J. TGA-DTA study on calcination of zeolitic catalysts. *Thermochim. Acta* **1997**, *294*, 39–44.

- (8) Vattipalli, V.; Paracha, A. M.; Hu, W.; Chen, H.; Fan, W. Broadening the Scope for Fluoride-Free Synthesis of Siliceous Zeolites. *Angew. Chem., Int. Ed.* **2018**, *57*, 3607–3611.
- (9) Iyoki, K.; Itabashi, K.; Okubo, T. Progress in seed-assisted synthesis of zeolites without using organic structure-directing agents. *Micropor. Mesopor. Mater.* **2014**, *189*, 22–30.
- (10) Meng, X.; Xiao, F.-S. Green Routes for Synthesis of Zeolites. *Chem. Rev.* **2013**, *114*, 1521–1543.
- (11) Goel, S.; Zones, S. I.; Iglesias, E. Synthesis of Zeolites via Interzeolite Transformations without Organic Structure-Directing Agents. *Chem. Mater.* **2015**, *27*, 2056–2066.
- (12) Nasser, G. A.; Muraza, O.; Nishitoba, T.; Malaibari, Z.; Al-Shammari, T. K.; Yokoi, T. OSDA-free chabazite (CHA) zeolite synthesized in the presence of fluoride for selective methanol-to-olefins. *Microporous Mesoporous Mater.* **2019**, *274*, 277–285.
- (13) Bajpai, P. K. Synthesis of mordenite type zeolite. *Zeolites* **1986**, *6*, 2–8.
- (14) Tanabe, K.; Hölderich, W. F. Industrial application of solid acid–base catalysts. *Appl. Catal. A: Gen.* **1999**, *181*, 399–434.
- (15) Moliner, M.; Martínez, C.; Corma, A. Multipore Zeolites: Synthesis and Catalytic Applications. *Angew. Chem., Int. Ed.* **2015**, *54*, 3560–3579.
- (16) Itabashi, K.; Fukushima, T.; Igawa, K. Synthesis and characteristic properties of siliceous mordenite. *Zeolites* **1986**, *6*, 30–34.
- (17) Zhang, L.; Xie, S.; Xin, W.; Li, X.; Liu, S.; Xu, L. Crystallization and morphology of mordenite zeolite influenced by various parameters in organic-free synthesis. *Mater. Res. Bull.* **2011**, *46*, 894–900.
- (18) Huang, X.; Zhang, R.; Wang, Z. Controlling Crystal Transformation between Zeolite ZSM-5 and Mordenite without Organic Structure-Directing Agent. *Chin. J. Catal.* **2012**, *33*, 1290–1298.
- (19) Zhu, J.; Liu, Z.; Endo, A.; Yanaba, Y.; Yoshikawa, T.; Wakihara, T.; Okubo, T. Ultrafast, OSDA-free synthesis of mordenite zeolite. *CrystEngComm* **2017**, *19*, 632–640.
- (20) Hesas, R. H.; Baei, M. S.; Rostami, H.; Gardy, J.; Hassanpour, A. An investigation on the capability of magnetically separable Fe<sub>3</sub>O<sub>4</sub>/mordenite zeolite for refinery oily wastewater purification. *J. Environ. Manage.* **2019**, *241*, 525–534.
- (21) Jain, R.; Rimer, J. D. Seed-Assisted zeolite synthesis: The impact of seeding conditions and interzeolite transformations on crystal structure and morphology. *Microporous Mesoporous Mater.* **2020**, *300*, No. 110174.
- (22) Shannon, M. D.; Casci, J. L.; Cox, P. A.; Andrews, S. J. Structure of the two-dimensional medium-pore high-silica zeolite NU-87. *Nature* **1991**, *353*, 417–420.
- (23) Petrovic, I.; Navrotsky, A.; Davis, M. E.; Zones, S. I. Thermochemical study of the stability of frameworks in high silica zeolites. *Chem. Mater.* **1993**, *5*, 1805–1813.
- (24) Liu, F.; Huang, K.; Zheng, A.; Xiao, F.-S.; Dai, S. Hydrophobic Solid Acids and Their Catalytic Applications in Green and Sustainable Chemistry. *ACS Catal.* **2017**, *8*, 372–391.
- (25) Hincapie, B. O.; Garces, L. J.; Zhang, Q.; Sacco, A.; Suib, S. L. Synthesis of mordenite nanocrystals. *Microporous Mesoporous Mater.* **2004**, *67*, 19–26.
- (26) Idris, A.; Khalil, U.; AbdulAziz, I.; Makertihartha, I. G. B. N.; Lanuwati, M.; Al-Betar, A.-R.; Mukti, R. R.; Muraza, O.; et al. Fabrication zone of OSDA-free and seed-free mordenite crystals. *Powder Technol.* **2019**, *342*, 992–997.
- (27) Velaga, B.; Peela, N. R. Seed-assisted and OSDA-free synthesis of H-mordenite zeolites for efficient production of 5-hydroxymethylfurfural from glucose. *Microporous Mesoporous Mater.* **2019**, *279*, 211–219.
- (28) Garg, N.; Skibsted, J. Dissolution kinetics of calcined kaolinite and montmorillonite in alkaline conditions: Evidence for reactive Al(V) sites. *J. Am. Ceram. Soc.* **2019**, *102*, 7720–7734.
- (29) De Witte, B. M.; Grobet, P. J.; Uytterhoeven, J. B. Pentacoordinated Aluminum in Noncalcined Amorphous Aluminosilicates, Prepared in Alkaline and Acid Mediums. *J. Phys. Chem.* **1995**, *99*, 6961–6965.
- (30) Kakihana, M.; Yoshimura, M. Synthesis and Characteristics of Complex Multicomponent Oxides Prepared by Polymer Complex Method. *Bull. Chem. Soc. Jpn.* **1999**, *72*, 1427–1443.
- (31) Baerlocher, C.; McCusker, L. B. Database of Zeolite Structures. <http://www.iza-structure.org/databases/> (accessed Jan 1, 2021).
- (32) Meunier, F. C.; Verboekend, D.; Gilson, J.-P.; Groen, J. C.; Pérez-Ramírez, J. Influence of crystal size and probe molecule on diffusion in hierarchical ZSM-5 zeolites prepared by desilication. *Microporous Mesoporous Mater.* **2012**, *148*, 115–121.
- (33) Farrusseng, D.; Tuel, A. Perspectives on zeolite-encapsulated metal nanoparticles and their applications in catalysis. *New J. Chem.* **2016**, *40*, 3933–3949.
- (34) Korányi, T. I.; Nagy, J. B. Distribution of Aluminum in Different Periodical Building Units of MOR and BEA Zeolites. *J. Phys. Chem. B* **2005**, *109*, 15791–15797.
- (35) Yu, Z.; Li, S.; Wang, Q.; Zheng, A.; Jun, X.; Chen, L.; Deng, F. Brønsted/Lewis Acid Synergy in H–ZSM-5 and H–MOR Zeolites Studied by <sup>1</sup>H and <sup>27</sup>Al DQ-MAS Solid-State NMR Spectroscopy. *J. Phys. Chem. C* **2011**, *115*, 22320–22327.
- (36) Haouas, M.; Taulelle, F.; Martineau, C. Recent advances in application of <sup>27</sup>Al NMR spectroscopy to materials science. *Prog. Nucl. Magn. Reson. Spectrosc.* **2016**, *94–95*, 11–36.
- (37) Engelhardt, G.; Fahlke, B.; Mägi, M.; Lippmaa, E. High-resolution solid-state <sup>29</sup>Si and <sup>27</sup>Al n.m.r. of aluminosilicate intermediates in zeolite A synthesis. *Zeolites* **1983**, *3*, 292–294.
- (38) Perras, F. A.; Wang, Z.; Kobayashi, T.; Baiker, A.; Huang, J.; Pruski, M. Shedding light on the atomic-scale structure of amorphous silica–alumina and its Brønsted acid sites. *Phys. Chem. Chem. Phys.* **2019**, *21*, 19529–19537.
- (39) Cundy, C. S.; Cox, P. A. The Hydrothermal Synthesis of Zeolites: History and Development from the Earliest Days to the Present Time. *Chem. Rev.* **2003**, *103*, 663–702.
- (40) Cundy, C. S.; Cox, P. A. The hydrothermal synthesis of zeolites: Precursors, intermediates and reaction mechanism. *Microporous Mesoporous Mater.* **2005**, *82*, 1–78.
- (41) Kumar, M.; Luo, H.; Román-Leshkov, Y.; Rimer, J. D. SSZ-13 Crystallization by Particle Attachment and Deterministic Pathways to Crystal Size Control. *J. Am. Chem. Soc.* **2015**, *137*, 13007–13017.
- (42) Soekiman, C. N.; Miyake, K.; Hirota, Y.; Uchida, Y.; Tanaka, S.; Miyamoto, M.; Nishiyama, N. Solvent/OSDA-free transformation of unseeded aluminosilicate into various zeolites via mechanochemical and vapor treatments. *Microporous Mesoporous Mater.* **2019**, *273*, 273–275.
- (43) Yoshizawa, K.; Kato, H.; Kakihana, M. Synthesis of Zn<sub>2</sub>SiO<sub>4</sub>:Mn<sup>2+</sup> by homogeneous precipitation using propylene glycol-modified silane. *J. Mater. Chem.* **2012**, *22*, 17272–17277.